

# Dispersion of mass by two-dimensional homogeneous and incompressible Çinlar flows

Mine Çağlar

*Koç University, Istanbul, Turkey*

## **Abstract**

We consider the dispersion of passive tracers in stationary, homogeneous and incompressible Çinlar flows on the plane. The associated velocity field is generated by the superposition of eddies of various size, arrival time and location which form a Poisson point process. Our focus is on the dispersion of a tracer cloud, which is measured through the variance of its centroid and the mean of the dispersion tensor. We also study single particle dispersion and particle pair separations in conjunction with dispersion. Monte Carlo simulations of all these measures first establish the relation of the dispersion to the parameters of the flow model. Second, the physical predictions on the behavior of these measures with respect to time as well as their relationship to each other are confirmed.

*Key Words:* Stochastic flow; Dispersion; Lagrangian velocity; Diffusivity; Mass transport.

## **1. Introduction**

The study of dispersion of inert solutes in water finds applications in oceanography [1] and ground water hydrology [2]. The solute is usually a pollutant such as crude oil or industrial waste dispersed by mainly by turbulent diffusion in the ocean or through mechanisms caused

by heterogeneity of the hydraulic properties in ground water. In this paper, we consider mass transport and dispersion by flows with Çinlar velocity fields [3,4]. Such velocity fields are vector field-valued versions of Poisson shot-noise and are close to those used in discrete vortex methods. By a more general definition of a vortex, they can be made homogeneous, incompressible and isotropic easily, and by construction they are stationary and ergodic.

In the last two decades, a significant amount of data has been collected especially in the ocean. The current following drifters are observed in several regions, some of which show the characteristics of stationary and homogeneous turbulence (e.g. [5]). These and other studies (e.g. [6]) indicate that the flow in the ocean is much more correlated in time than a random walk or a Brownian flow. Çinlar flows can model medium-scale structures of motion through significant correlations in time as opposed to small-scale structures usually modeled by a Brownian flow. In Brownian flows, the particle paths have independent increments whereas in Çinlar flows the velocity field has independent increments to yield medium-term to long-term correlated particle paths.

We focus on horizontal dispersion in  $R^2$ , in view of the applications where vertical diffusion makes no significant contribution to the spread of pollutants. Several measures of dispersion are considered; namely, single particle dispersion, the centroid and relative dispersion tensor, and particle pair separations. The entire cloud of mass, or tracer, determines the centroid and dispersion tensor whereas particle statistics can be related to these measures.

Stationary and homogeneous turbulence is assumed as well as incompressibility, and this property is the basis of asymptotic computations in single particle dispersion. Particle pair separations, the centroid and relative dispersion tensor involve more complicated correlations

of the velocities than single particle dispersion and are hard to evaluate analytically. We study these by Monte Carlo simulations and compare with the physical arguments and predictions for such measures. We have previously established the dependence of the eddy diffusivity as derived from single particle dispersion on the typical time scale, which is defined through the parameters of the velocity model [7]. In the present study, we also compute the particle pair diffusivity and the effective dispersion constant from the dispersion tensor and compare with the eddy diffusivity.

The organization of the paper is as follows. We review the flow model and its properties in Section 2. Various measures of dispersion are discussed in Section 3. In Section 4, our results of Monte Carlo simulations are presented and compared with previous results on single particle dispersion. Finally, Section 5 includes the conclusions of this study.

## 2. Flow Model

Flow with a velocity field  $u$  arises as the set of solutions to the ordinary differential equation

$$\frac{d}{dt}X_t = u(X_t, t), \quad X_0 = x \quad (1)$$

while  $x$  varies in  $R^d$ . We consider the homogeneous Çinlar velocity field [3,4] on  $R^d$ . As building blocks of the velocity field, various eddies or vortices are obtained by

$$a v\left(\frac{x-z}{b}\right) \quad (2)$$

where  $z \in R^d, a \in R, b \in (0, \infty)$  and  $v$  is a deterministic velocity field called the *basic vortex* or *eddy*. A new eddy is obtained from the basic eddy  $v$  through amplification with  $a$ , translation with  $z$  and dilation with  $b$ .

The velocity field is constructed as the superposition of variable size eddies, which arrive according to a Poisson process and decay exponentially in time. In particular with  $d=2$ , it is given by

$$u(x, t) = \int_{-\infty}^t \int_Q N(ds, dz, da, db) e^{-c(t-s)} a v\left(\frac{x-z}{b}\right) \quad x \in R^2, t \in R \quad (3)$$

where  $N$  is a Poisson random measure on the Borel sets of  $R \times Q$ , with  $Q = R^2 \times R \times (0, \infty)$  and  $c > 0$  is a decay parameter. The mean measure of  $N$  is crucial in establishing homogeneity in space [4], given by

$$\mu(dt, dz, da, db) = \lambda dt dz \alpha(da) \beta(db) \quad (4)$$

where  $\lambda$  is the arrival rate of eddies per unit time-unit space, and  $a$  and  $b$  are probability distributions. The variables  $z$ ,  $a$ ,  $b$  as well as the time of arrival  $t$  of each eddy are all governed by the Poisson random measure  $N$ .

The motivation behind the velocity field  $u$  comes from the observations of eddies in the ocean which seem to occur sporadically in time rather than continuously. A Poisson process captures arrivals that occur in this manner: independent from each other and one at a time. In view of this and with the aim of constructing a non-Gaussian velocity field, a Poisson random measure is used to construct  $u$  as opposed to a white noise that appears in the constructions based on stochastic differential equations [3].

The velocity field (3) has independent increments and hence is a Markov process. The exponential decay coefficient in (3) guarantees the Markovian property, which facilitates a more tractable analysis of the velocity field and its Lyapunov exponents. Nevertheless, the Markov velocity field  $u$  yields medium-term to long-term correlated particle paths consistent with Lagrangian observations of the ocean. In contrast, the particle paths are Markovian in a

Brownian flow and indicate short term correlation. Therefore, a flow model based on a Markov velocity field represents real oceanic flows more accurately and can be considered as a one step generalization of a Brownian flow (see also Refs. [8,9]).

In view of the observations, we consider eddies of rotational form [7]. The basic eddy is a rotation in two dimensions with center at the origin and support on the unit disk. That is,

$$v^1(x) = -\frac{x^2}{r}m(r), \quad v^2(x) = \frac{x^1}{r}m(r) \quad x = (x^1, x^2), \quad r = |x| \in [0,1] \quad (5)$$

where  $m(r)$  is the magnitude of the rotation at distance  $r$ . As a rotation in  $R^2$ ,  $v$  is divergence free and is invariant under rotations. An arbitrary eddy is also a rotation, but with center at  $z$  and radius  $b$ ,  $z \in R^2$ ,  $b \in (0, \infty)$ . Therefore,  $u$  is also divergence free and its distribution is invariant under rotations. Hence, the flow is incompressible as well as isotropic. Finally, the velocity field is strictly stationary in time due to its construction as in (3) [3]. For a review of such properties, see [7].

In this paper, the distribution  $b$  of the radius  $b$  is taken to be the same distribution as in previous studies in order to compare the single particle dispersion obtained earlier in [7] with the dispersion results of the present study. It is set to be a discrete distribution with the probability mass function

$$p(0.5) = 8/15, \quad p(1) = 4/15, \quad p(1.5) = 2/15, \quad p(2) = 1/15. \quad (6)$$

Accordingly, most eddies are small and only a few are large in size as observed in the ocean. Turbulence is characterized by a large spectrum of eddy sizes. However in simulations, a cut off value is needed from above in order to have only finite number of eddies affecting the particle at any time. With this limitation, a continuous distribution on the interval  $[0,2]$  could be a more general alternative of (6). The choice of the upper limit 2 is arbitrary, yet the other

simulation parameters are varied in a wide range accordingly and the particles are tracked sufficiently long so that the dispersion behavior is observed. In fact, we have run trial simulations with a truncated form of a Pareto distribution, which is continuous and also represents many small and a few large eddies. Since the qualitative results aimed in this study have not changed, we have continued with distribution (6) for comparison purposes.

Similarly, the distribution  $a$  of the amplitude  $a$  is set to be a uniform distribution over an interval as before. The magnitude function  $m$  is taken to be a smooth continuous function. Previously, it has been found that a variety of particle motions can be generated by the change of parameters  $l$ ,  $c$  and the support of  $a$  [7]. Single particle dispersion depends on a time scale defined as a function of these parameters. On the other hand, the largest Lyapunov exponent depends on the same time scale and is strictly positive as expected in a turbulent flow [10]. Existence of Lyapunov exponents depends on the smoothness of  $m$ , which is taken to vanish at the origin and at the boundary of a vortex for this reason.

### 3. Measures of Dispersion

In this section, we quantify the translation and the spread of a passive tracer in a flow through various identifiers. The common concept to all is the concentration of mass defined as the mass of solute per volume of fluid surrounding each point. Let the total mass of a tracer cloud be  $M$  and let  $c(x,t)$  denote the concentration of mass at position  $x$ , at time  $t$ . That is,  $M = \int c(x,0) dx$ , and we have  $M = \int c(x,t) dx$ , for all  $t \geq 0$ , by conservation of mass. The evolution of  $c$  in space and time is the main concern of transport studies.

The stationarity, homogeneity and incompressibility properties play an important role on the identification of several measures of dispersion. In general, the Lagrangian velocity is defined as the entire velocity field viewed from the position of a moving particle in the flow. In particular, we refer to the process  $\{u(X_t, t) : t \neq 0\}$ , the velocity of a diffusing particle, as the Lagrangian velocity. In stationary and homogeneous turbulence, the Lagrangian velocity is considered to be a stationary process by physical arguments. Taylor's theorem [11] has been used in this case for analysis of, especially, single particle dispersion [12,13,14,15]. The mathematical proof of this fact, however, requires the incompressibility property and is relatively new [16,17,18,19]. With incompressibility, it can be shown that the Lagrangian velocity is both stationary and has the same distribution as the Eulerian velocity for each fixed time  $t$ . See [20] for a full account and related new results.

### 3.1 Spatial moments of concentration: center of mass and dispersion tensor

At time  $t$ , the *center of mass* of the tracer cloud is given by

$$C_t = \frac{1}{M} \int_{R^2} x c(x, t) dx \quad (7)$$

and the *dispersion tensor* is defined as

$$D_t = \frac{1}{M} \int_{R^2} (x - C_t)(x - C_t)^T c(x, t) dx . \quad (8)$$

The statistical moments of  $C_t$  and  $D_t$  cannot be computed analytically for many flow models.

As a special case, in the case of homogeneous and incompressible turbulence, the mean of the centroid at time  $t$ ,  $EC_t$ , can be computed as

$$EC_t = \frac{1}{M} E \int_{R^2} x c(x, t) dx = \frac{1}{M} \int_{R^2} E[X_t(x)] c(x, 0) dx = \frac{1}{M} \int_{R^2} (x + \bar{u}t) c(x, 0) dx = C_0 + \bar{u}t \quad (9)$$

where  $\bar{u}$  is the mean of the Eulerian velocity (3). Here, we use the fact that

$$EX_t(x) = x + \int_0^t Eu(X_s, s) ds = x + \bar{u}t \quad \text{and the expected value of the Lagrangian velocity is}$$

equal to  $\bar{u}$  due to its stationarity. Note that  $\bar{u}$  is a constant in stationary, homogeneous and incompressible turbulence [20]. That is, the center of the cloud is translated with the mean flow. On the other hand, the variance of  $C_t$ , or equivalently its second moment  $EC_t C_t^T$  when  $\bar{u}$  is chosen 0 without loss of generality, is an indicator of dispersion. Similarly,  $ED_t$  is another measure of dispersion since  $D_t$  is itself a second order quantity. It indicates the dispersion of mass with respect to its center  $C_t$ . It is easy to show that these two indicators are related by

$$ED_t = E \frac{1}{M} \int_{R^2} \mathbf{x} \mathbf{x}^T c(\mathbf{x}, t) d\mathbf{x} - EC_t C_t^T = \frac{1}{M} \int_{R^2} \mathbf{x} \mathbf{x}^T \bar{c}(\mathbf{x}, t) d\mathbf{x} - EC_t C_t^T \quad (10)$$

where  $\bar{c}$  denotes the mean concentration field. The first term in the right hand side of (10) can be interpreted as the *absolute dispersion* and is the sum of the *relative dispersion*  $ED_t$  and the *meandering*  $EC_t C_t^T$ .

Although the relative dispersion is defined slightly different in [21], the relationship (10) is assumed to hold for that definition as well with the same absolute dispersion and meandering. There, it is predicted by physical arguments that when relative diffusion is dominated by eddies in the inertial subrange, that is, when the cloud size is comparable in size to these eddies, the cloud size grows faster than linearly with time. Equivalently, the relative dispersion  $ED_t$  is expected to grow like  $t^2$ . This is much faster than the linear growth seen in molecular diffusion. The duration of this ‘‘explosive phase’’ is expected to be rather short, in fact, shorter than the lifetime of the typical energy containing eddy in the field. When a cloud becomes large compared to the energy containing eddies, it is predicted to grow linearly with time as in

molecular diffusion although the following measure of diffusivity

$$\frac{1}{2} \frac{dED_t}{dt} \quad (11)$$

would be much larger than the molecular diffusivity. In this regime, the cloud is expected to forget its initial position and to behave as if discharged from a point source. By this discussion, the cloud size, which is defined as  $\sqrt{D_t^{ii}}$ ,  $i=1,2$ , would grow as the point-source cloud. The relationship of single particle dispersion and point-source cloud is pointed out in the next subsection.

In the ground water hydrology context, Dagan [2] suggests (11) as the definition of the *effective dispersion coefficient* a term which makes sense when it becomes a constant for large  $t$ . This will be one of the indicators used in our computations rather than  $D_t$  itself, which is only a random quantity.

### 3.2 Single particle dispersion

The probability that a particle is found at  $x$  at time  $t$  can be heuristically identified with the mean concentration of a diffusing tracer cloud at that position and time. The basis of this identification lies in the assumption that all particles diffuse independently, an assumption which is only approximate for oceanic flows. Then, when a large ensemble of particles is released at the origin at time 0 (a point-source cloud), the amount of mass at  $x$  at time  $t$  would be proportional to the desired probability. By this argument, the absolute dispersion that appears in (10) is linked to the second moment of a single particle position at each time  $t$ .

Let  $X_t$  be the position of a particle at time  $t$ , which started at position 0 at time 0. The *single particle dispersion* can be defined as the mean square particle position

$$E|X_t|^2 = E(X_t^1)^2 + E(X_t^2)^2 . \quad (12)$$

For a homogeneous and incompressible flow, (12) grows quadratically in  $t$  initially and linearly as  $t \rightarrow \infty$  [12,21]. The proof of this result relies on the stationarity of the Lagrangian velocity which can be shown by the incompressibility and homogeneity properties [20]. When the distribution of  $X_t$  is assumed to be Gaussian, the diffusion constants in the advection-diffusion equation for the mean concentration are found as

$$K^{ii} = \frac{1}{2} \frac{d}{dt} E(X_t^i)^2 \quad i=1,2 \quad (13)$$

when molecular diffusion is neglected [21, pg.62]. In general, the scalar quantity  $K \equiv K^{11} = K^{22}$  is taken as a definition for *eddy diffusivity* in isotropic and stationary turbulence if the cross covariances  $E(X_t^i X_t^j)$ ,  $i \neq j$ , are negligible [12, pg.500]. If the flow is not isotropic or the cross covariances are also to be investigated, the diffusivity is defined as a tensor  $[K^{ij}]$  [1, pg.57]. As our flow model is isotropic, we concentrate on the diagonal entries only and consider the scalar definition of  $K$  which is a constant as  $t \rightarrow \infty$ .

### 3.3 Particle Pair Separation

The diffusion of a tracer cloud with respect to its center of mass is closely linked to the rate at which two particles separate in a flow as exploited by Batchelor [22]. The second moment of the concentration of a tracer cloud can be identified with the joint probability density of the position of a particle pair as an experimental approximation, in the same way as the mean of the concentration of a cloud is identified with the probability density of a single particle [21]. It

follows from this argument that the mean square separation of a diffusing particle pair is just twice the mean square dispersion with respect to the center of mass. Therefore, the drifting particle pairs provide experimental information on the relative diffusion of a tracer cloud about its center of mass.

Let  $X_t$  and  $Y_t$  be the positions of two particles at time  $t$  that started to drift at a distance  $s$  from each other at time 0. The particle pair separation at time  $t$  is given by  $|X_t - Y_t|$ . We are interested in the mean square particle separation

$$E|X_t - Y_t|^2 = E(X_t^1 - Y_t^1)^2 + E(X_t^2 - Y_t^2)^2 . \quad (14)$$

To investigate the rate of growth of (14) for various initial separations  $s$ , we consider the standardized quantity

$$Z(t) = E|X_t - Y_t|^2 - s^2 . \quad (15)$$

Following the ideas of Richardson [23], qualitative predictions can be made [21]. For a particle pair, turbulent eddies large compared to particle separation move them about together. On the other hand, eddies small compared to the separation affect this distance relatively little. Most effective are eddies of a size comparable to the separation distance itself. Since the separation grows in time, after a while the separation distance becomes much larger than the largest eddy present in the flow. In that case, the relative motion of two particles is expected to resemble the motion of a single particle in a homogeneous field of turbulence.

#### 4. Computational Results

The dispersion measures introduced in the previous section are investigated through Monte Carlo simulations in this section. Since the single particle dispersion has been studied in detail

in [7], we consider the spatial moments of concentration of a cloud of passive tracer and particle pair separations in the computations. Our aim is twofold: first to examine the behavior of these measures and compare them with those predicted by physical insight, and, second to link this behavior with the parameters of the flow model.

Previous studies [7,10] show that the parameters of the model can be changed through varying a certain time scale, called the typical time, to span a wide range of behaviors of the physical quantities defined on the flow. In order to introduce the typical time, we first define a *length scale*  $l$ . Converting the definition in Ref. [24] which is based on spectral density to a definition in terms of covariance, we get [7]

$$l = \left( \frac{R^{11}(0,0) + R^{22}(0,0)}{-[\partial_1^2(R^{11}(x,0) + R^{22}(x,0)) + \partial_2^2(R^{11}(x,0) + R^{22}(x,0))]_{x=0}} \right)^{1/2} \quad (16)$$

where  $\partial_i^2 \equiv \partial^2 / \partial x_i^2$  is the second partial derivative operator with respect to space and

$$R^{ij}(x,t) = E u^i(y,s) u^j(y+x,t+s) \quad x, y \in R^2, s, t \in R, i, j=1,2.$$

That is,  $R$  being the covariance tensor is a function of the space lag  $x$  and the time lag  $t$  due to homogeneity and stationarity of  $u$ , respectively. In (16), units of 'velocity squared' is divided by units of '1/(time squared)', and then the square root is taken, so  $l$  is in units of length. In [24],  $l$  is called the correlation radius as it inherits the correlation information. Another way of defining a length scale could be by taking the partial derivative of  $R$ , which is in units of 'velocity squared', only once to have a quantity in units of 'acceleration', and then dividing  $R$  by this to get a quantity in units of 'length'. See for example, Ref. [25, pg.51]. Other definitions using spatial correlations as above can be found in [13] where physical aspects are also discussed. However, our definition (16) takes advantage of isotropy and the quantities are simpler to evaluate. As shown in [4],

$$R^{ij}(x,t) = \frac{1}{2c} e^{-c|t|} \lambda \int_R \alpha(da) a^2 \int_{R_+} \beta(db) b^2 \int_{R^2} dz v^i(z) v^j(z+x/b) \quad (17)$$

and from (5) we get

$$l = \left( \frac{\int \beta(db) b^2 \int_0^1 dr r m^2(r)}{-\int_0^1 dr r m(r) [m''(r) + m'(r)/r - m(r)/r^2]} \right)^{1/2} \quad (18)$$

The details of this derivation can be found in [7]. Note that (18) is determined by the distribution  $b$  of (6) and the magnitude function  $m$ , which is taken to be  $m(r) = (1 - \cos 2\pi r)/2$ ,  $0 \leq r \leq 1$  here. As a result,  $l$  is computed to be 0.235 length units. The simulations below continue until all the dispersion quantities are computed. This amounts to tracking the particles in a radius of 5 to 20 length units depending on the other parameters of the model.

The *typical time*  $\tau$  is defined as the ratio of the length scale  $l$  to the typical velocity

$$\sqrt{E|u(0,0)|^2} \equiv (E[(u^1(0,0))^2 + (u^2(0,0))^2])^{1/2} = [R^{11}(0,0) + R^{22}(0,0)]^{1/2}. \quad (19)$$

Since we have [7]

$$R^{11}(0,0) + R^{22}(0,0) = \frac{\lambda\pi}{c} \int \alpha(da) a^2 \int \beta(db) b^2 \int_0^1 dr r m^2(r) \quad (20)$$

the typical time  $\tau$  is found as

$$\begin{aligned} \tau &= \frac{l}{[R^{11}(0,0) + R^{22}(0,0)]^{1/2}} \\ &= \left[ -\frac{\lambda\pi}{c} \int \alpha(da) a^2 \int_0^1 dr r m(r) [m''(r) + m'(r)/r - m(r)/r^2] \right]^{-1/2} \end{aligned} \quad (21)$$

Here, we vary  $t$  from 0.01 to 10 to span a wide range of parameters in the simulations by changing the parameters  $l$ ,  $c$  and the support of  $a$ . The ratio  $l/c$  for fixed  $t$  has been found to affect the duration of the small time behavior and the value of the diffusivity in single particle dispersion [7]. The eddy diffusivity is a nondecreasing function of the ratio  $l/c$ . However, the change in the magnitude of the diffusivity with respect to  $l/c$  is insignificant compared to that with respect to  $t$ . The small-time behavior of single particle dispersion is encountered until about  $10t$  for intermediate and larger values of  $l/c$ ; for smaller values it is observed until about  $5t$ . After this time, the large time linear behavior is observed. It has been shown that both the eddy diffusivity and the largest Lyapunov exponent decrease as the time scale  $t$  increases [7,10].

#### 4.1 Centroid and dispersion tensor

We consider a tracer cloud which is contained in a disk of unit radius around the origin with the initial concentration  $c(x,0)$  equal to 1 for all  $x \in R^2$ . Because of incompressibility, the constant concentration areas in the flow only change shape and the initial concentration remains the same within the boundary. Hence a deterministic and constant concentration does not represent  $c$ , but can be considered as an approximating region of a cloud of variable concentration in space. Hence, we can focus on the shape and distortion of a cloud as would be in an incompressible flow. An example of a sequence of snapshots of the mass is given in [7] for one realization.

The simulation procedure explained in detail in [7] is based on the integration of flow equation (1) through the fourth order Runge-Kutta method while the random velocity field is constructed as needed. For each set of parameters, an integration time step is chosen so that it

is the largest value for which the particle paths are invariant through the simulation horizon. Here, we start to follow 1000 particles on the boundary of the mass cloud, and as they separate fast in time, we insert new particles in between. The mass is contained within the boundary at all times since the flow is a homeomorphism and the area of the cloud remains the same due to incompressibility. As a result, also the concentration remains the same within the boundary. The length of the boundary, hence the number of particles followed, grows exponentially fast as the largest Lyapunov exponent of this flow is empirically found to be positive [10]. On the other hand, the generation of the velocity field being based on the simulation of a Poisson process is very fast. The bulk of the computation is on the deterministic integration of the particle paths.

At any time, we find the centroid and the dispersion by a line integral over the boundary using Green's theorem. The insertion of new particles in time makes this calculation as precise as possible. As a supplementary measure, we find the radius of the minimal circle that encapsulates the cloud of tracer, which is centered at the origin. Since the initial tracer is released as centered at the origin, this is more relevant in applications such as the diffusion of a pollutant on the surface of the ocean or in ground water. One would like to know how this radius grows away from the initial site of the pollution, that is, the origin. The radius at time  $t$  is given by

$$R_t = \max \{|X_t(x)| : x \in B(t)\} \quad (22)$$

where  $B(t)$  is the boundary of the cloud at time  $t$ . In contrast, the dispersion relative to the centroid is studied through  $D_t$ .

We have computed  $ER_t$ , and the traces of the matrices  $EC_t C_t^T$  and  $ED_t$ , denoted by  $E|C_t|^2$  and  $\text{tr}ED_t$ , in the following computations. These computations also show minor dependence on  $l/c$

as in single particle dispersion. Therefore, we report only the case  $l/c=1$  here to demonstrate the relation of dispersion to the parameters of the model. A similar relation holds for other values of  $l/c$ . Monte Carlo simulation is performed with 1000 independent replications. The means of the traces of the matrices  $C_t C_t^T$  and  $D_t$  are found over this sample of 1000. As the estimators of the traces of  $EC_t C_t^T$  and  $ED_t$ , respectively, we find

$$\overline{|C_t|^2} = \overline{(C_t^1)^2} + \overline{(C_t^2)^2} \quad (23)$$

$$\overline{\text{tr} D_t} = \overline{D_t^{11}} + \overline{D_t^{22}} \quad (24)$$

where  $\bar{X} = (\sum_{i=1}^{1000} X_i) / 1000$  is the sample mean of  $X$ .

The results are given in Figures 1 to 3. We see that both the variance of the centroid and the relative dispersion along the coordinate axes grow faster than linearly at small times and linearly at large times. These are important empirical results since both  $EC_t C_t^T$  and  $ED_t$  involve covariance terms like  $E u(X_s(x), s) u^T(X_r(y), r)$ ,  $r \leq t$ , whose structure is not known analytically. For example,

$$\begin{aligned} EC_t C_t^T &= E \frac{1}{M^2} \iint X_t(x) X_t^T(y) c(x, 0) c(y, 0) dx dy \quad (25) \\ &= E \frac{1}{M^2} \iint \int_0^t \int_0^t u(X_s(x), s) u^T(X_r(y), r) c(x, 0) c(y, 0) dr ds dx dy + EC_0 C_0^T \\ &= \frac{1}{M^2} \iint \int_0^t \int_0^t E[u(X_s(x), s) u^T(X_r(y), r)] c(x, 0) c(y, 0) dr ds dx dy + C_0 C_0^T \end{aligned}$$

where we use the equality  $C_t = \frac{1}{M} \int X_t(x) c(x, 0) dx$  because of conservation of mass, and the fact that the mean of the Lagrangian velocity is 0 like that of the Eulerian velocity. On the other hand, the behavior of single particle dispersion is known because it involves only

Lagrangian velocity moments, which are the same as those of the Eulerian velocity due to stationarity, homogeneity and incompressibility.

For Brownian flows, the asymptotic growth rates of  $E|C_t|^2$  and  $\text{tr}ED_t$  are linear or slower than linear in  $t$ , such as  $\log t$  and  $\sqrt{t}$ , depending on the largest Lyapunov exponent and the space dimension  $d$  [26]. In isotropic, homogeneous and incompressible Brownian flows, for  $d=2$ ,  $E|C_t|^2$  grows much slower than  $\log t$ , and  $\text{tr}ED_t$  grows linearly with  $t$  as  $t \rightarrow \infty$ . In contrast, in Çinlar flows, the growth of  $\text{tr}ED_t$  appears to be quadratic initially, and then becomes linear in  $t$ , exactly as expected by the physical arguments discussed above. Moreover, meandering is much stronger in Çinlar flows than in Brownian flows.

The mean radius  $ER_t$ , estimated by  $\overline{R_t}$  shown in Figure 3 grows rather slowly at first, and then increases linearly at large times. Although the meandering, that is, the variance of the centroid is strong, the mean radius  $ER_t$  grows slowly as the mean of the centroid is in fact 0 for all times. Probably, incompressibility plays a role on this outcome. With the area of the cloud also increasing in a compressible flow, the radius can possibly grow faster.

The results for  $t = 0.01, 0.1, 1, 10$  are all similar to each other. The graphs are almost the same except for the change in the scale of the time axis due to the different parameter sets corresponding to different  $t$ . This difference is quantified through the effective dispersion constant

$$K_d = \frac{1}{4} \frac{d}{dt} \text{tr}ED_t \quad \text{as } t \rightarrow \infty \quad (26)$$

in view of (11). Table 1 summarizes the results. As  $t$  increases, the effective dispersion constant decreases rapidly. This agrees with the intuition that for larger  $t$ , a fixed distance is traveled much more slowly by the particles and, hence, the dispersion constant is smaller.

We consider the scalar definition of the eddy diffusivity  $K$  ( $=K^{11}=K^{22}$  in (13)) and compute by

$$K = \frac{1}{4} \frac{d}{dt} E |X_t|^2 \text{ for large } t, \text{ in view of equations (12) and (13).}$$

The single particle dispersion and the dispersion of a tracer cloud for large times are very close in magnitude, which are measured by the eddy diffusivity  $K$ , and the effective dispersion constant  $K_d$ , respectively. This is in agreement with physical intuition that, for large times, the cloud size will grow as the point-source cloud, which can be identified with the dispersion of a single particle as explained before. The various values of  $K$  that were computed in [7] and here as well are also given in Table 1 for comparison.

#### 4.2 Particle pair separations

We start with a range of initial separations for several particle paths and plot the standardized separation squared  $Z(t)$  of (15). The initial separations are  $s=0.2,0.4,0.6,\dots,2$  length units; equivalently, approximately 1 length scale to 10 length scales  $l$  as given in (16), which is fixed to be 0.235 length units. Figure 4 gives the plot of  $Z(t)$  against time for all parameter combinations we have studied. As before, this is in fact an estimate of  $Z(t)$  as we find  $\overline{|X_t - Y_t|^2}$  over 1000 replications as an estimate of  $E|X_t - Y_t|^2$  given in (15).

In all cases, two conclusions can be drawn. First, the separation grows quadratically at the beginning, then linearly as  $t$  gets large. This is similar to the behavior of single particle

dispersion. Second,  $Z(t)$  coincides for the particle pairs that have initial separations more than or equal to  $6l$ , that is, about 1.4 length units in our setting. In view of the distribution of the radius  $b$ , this observation can be explained as follows. In order to affect both particles, at least in the initial stage, an eddy must have a radius of at least  $1.4/2=0.7$ . The radius  $b$  takes a value greater than 0.7 with only a probability of 0.5 and only a portion of such eddies are located so that both particles get affected by the same eddy. Hence, with a separation of at least 1.4 units, chances are that the particles move rather independently from each other, especially after they diffuse to large distances following their initial release. This is in agreement with the qualitative predictions about the eddy sizes and the separation of particles discussed in Section 3. Indeed, for large separations, we expect the motion of two particles to resemble the motion of a single particle.

Infinite separation is studied through single particle statistics in accordance with Richardson's ideas. For large separations, the mean square particle pair separation is expected to converge to the single particle variance. Davis [27] simulates the particle pair separation on a Gaussian velocity field. There, all the initial separations considered are relatively small since the curves for  $Z(t)$  are far away from the curve for two infinitely separated particles. Hence, convergence of  $Z$  to the value corresponding to a single particle behavior was not achieved.

In our case, we are able to find the critical separation as  $6l$ , above which particles diffuse as if they are infinitely separated as observed in Figure 4. In analogy with particle separation in pure diffusion, the *particle pair diffusivity* can be defined [27] as

$$K_p = \frac{1}{8} \frac{d}{dt} E|X_t - Y_t|^2 = \frac{1}{8} \frac{d}{dt} Z(t). \quad (27)$$

Of course,  $K_p$  depends on the initial separation, and for each fixed initial separation, it is a constant only for large  $t$ . Here, we compute  $K_p$  only for large separations,  $6l$  and above, and compare it with the single particle diffusivity  $K$  in Table 2. We see that the  $K$  ( $=K^{11}=K^{22}$  by isotropy), which have been computed in [7], are approximately equal to  $K_p$ .

Finally, Figure 5 shows the log-log plot of the effective dispersion constant  $K_d$  and the particle pair diffusivity  $K_p$  together with respect to the time scale  $t$ . The eddy diffusivity  $K$ , both  $K_d$  and  $K_p$  decrease as  $t$  increases.

## 5. Conclusions

In this paper, we have investigated the behavior of the dispersion of a tracer cloud in a stationary, homogeneous, and incompressible Çinlar velocity field. This velocity field models the medium-scale structures of motion observed in the ocean as opposed to the molecular level or small-scale motion usually modelled by Brownian or Gaussian type flows. The dispersion of a cloud is measured through relative dispersion matrix with respect to the centroid. Another indicator of dispersion is the meandering of the centroid. These measures, particle pair separations and the minimum radius that encapsulates the cloud are all computed as functions of time for a range of parameters that span several time scales.

This work demonstrates the interplay between several measures of dispersion on a stationary, homogeneous and incompressible velocity field. Physical arguments provide insight to the behavior of dispersion matrix and particle pair separations. However, for more involved models such as Çinlar flows, cross correlations of the Lagrangian velocities cannot be computed analytically. Hence, the behavior of the dispersion measures, which involve such

correlations, cannot be predicted mathematically. Instead, we have pursued a thorough Monte Carlo simulation analysis to do the computations. The physical predictions are confirmed by this analysis for a wide range of parameters.

The nature of time dependence of the dispersion measures is established. Our results show that both relative dispersion and the variance of the centroid grow quadratically at first, and then linearly for large times as in the case of the single particle dispersion. The large time linear relationship is used to quantify the relative dispersion of the mass cloud through an effective dispersion constant and is compared with the single particle dispersion through the eddy diffusivity. We find that, for large times, the effective dispersion constant and the eddy diffusivity are very close in magnitude. This observation is consistent with the physical prediction that for large times, the tracer cloud grows like the point-source cloud, which, in turn, is related to the single particle dispersion.

The relation of the effective dispersion constant to the parameters of the velocity model is also determined. The effect of the parameters can be summarized through a composite one, namely the typical time scale. As the time scales increases, the effective dispersion decreases. Intuitively, as the time to traverse the typical length increases, the rate of dispersion slows down.

The drifting particle pairs provide experimental information on the relative diffusion of a tracer cloud about its center of mass. Therefore, we have traced several particle separations in time. The change of the separations in time is in accordance with physical insight. As the initial separation increases, the particle pair behaves like a single particle, because, then, the

separation is greater than the largest eddy present in the flow. This fact is also quantified by the comparison of the particle pair diffusivity constant with the single particle diffusivity.

**Acknowledgement.** The author would like to thank anonymous referees for their detailed comments that improved the presentation of this work.

## References

- [1] R.E. DAVIS (1991) Lagrangian Ocean Studies. *Annu. Rev. Fluid Mech.*, **23**: 43-64.
- [2] G. DAGAN (1990) Transport in Heterogeneous Porous Formations: Spatial Moments, Ergodicity, and Effective Dispersion. *Water Resources Research*, **26**: 1281-1290.
- [3] E. ÇINLAR (1993) On a Random Velocity Field. Technical report, Princeton University, Princeton, NJ.
- [4] E. ÇINLAR (1994) Isotropic Velocity Fields of Poisson Shot Noise Type. Technical report, Princeton University, Princeton, NJ.
- [5] R. HAYNES and E.D. BARTON (1991) Lagrangian Observations in the Iberian Coastal Transition Zone. *J. Geophys. Res.*, **96**: 14731-14741.
- [6] P.S. ADDISON (1996) A method for Modelling Dispersion Dynamics in Coastal Waters Using Fractional Brownian Motion. *Journal of Hydraulic Research*, **34**: 549-561.
- [7] M. ÇAĞLAR (2000) Simulation of Homogeneous and Incompressible Çinlar Flows. *Appl. Math. Modelling*, **24**: 297-314.
- [8] R.A. CARMONA, S.A. GRISHIN and S.A. MOLCHANOV (1995) Massively Parallel Simulations of the Transport Properties of Gaussian Velocity Fields. In *Mathematical Models for Oceanography*. R.Adler, P.Muller, B.Rozovskii eds., Birkhauser, Boston.
- [9] L.I., PITERBARG (2001) The top Lyapunov exponent for a stochastic flow modeling the upper ocean turbulence. *SIAM J.Appl. Math*, **62**: 777-800.

- [10] M. ÇAĞLAR and E. ÇINLAR (2001) Lyapunov Exponents of Poisson Shot-Noise Velocity Fields. *Stochastic Processes and their Applications*, **94**: 29-49.
- [11] G.I. TAYLOR (1921) Diffusion by Continuous Movements. *Proc. London Math. Soc.*, **A 20**: 196.
- [12] S.B. POPE (2000) *Turbulent Flows*. Cambridge University Press, Cambridge.
- [13] J. MATHIEU and J. SCOTT (2000) *An Introduction to Turbulent Flow*. Cambridge University Press, New York.
- [14] K. BEVEN, P. CHATWIN and J. MILLBANK, Eds. (1994) *Mixing and Transport in the Environment*. Wiley, Chichester, England.
- [15] M.M. STANISIC (1988) *The Mathematical Theory of Turbulence*. Springer-Verlag, New York.
- [16] J.L. LUMLEY (1962) The Mathematical Nature of the Problem of Relating Lagrangian and Eulerian Statistical Functions in Turbulence. In *Mécanique de La Turbulence*. (Colloque International du CNRS à Marseille.) Editions du CNRS, Paris.
- [17] H. OSADA (1982) Homogenization of Diffusion Processes with Random Stationary Coefficients. *Proceedings of Fourth Japan-USSR Symposium on Probability Theory. Lecture Notes in Math.* **1021**: 507-517. Springer, Berlin.
- [18] S.C. PORT and C.J. STONE (1976) Random Measures and their Application to Motion in an Incompressible Fluid. *J. Appl. Probab.*, **13**: 498-506.
- [19] C.L. ZIRBEL (1993) Stochastic Flows: Dispersion of a Mass Distribution and Lagrangian Observations of a Random Field. Dissertation, Princeton University, Princeton, NJ.
- [20] C.L. ZIRBEL (2001) Lagrangian Observations of Homogeneous Random Environments. *Advances in Applied Probability*, **33**: 810-835.
- [21] G.T. CSANADY (1973) *Turbulent Diffusion in the Environment*. D. Reidel Pub. Co., Netherlands.

- [22] G.K. BATCHELOR (1952) Diffusion in a Field of Homogeneous Turbulence, II. The Relative Motion of Particle. *Proc. Cambridge Phil. Soc.*, **48**: 345-362.
- [23] L.F. RICHARDSON (1926) Atmospheric Diffusion on a Distance-Neighbor Graph. *Proc. Roy. Soc. London*, **A 110**: 709-737.
- [24] L.I., PITERBARG (1997) Short-Correlation Approximation in Models of Turbulent Diffusion. *Stochastic Models in Geosystems*. Springer-Verlag, New York.
- [25] A.J. CHORIN (1994) *Vorticity and Turbulence*. Springer-Verlag, New York.
- [26] C.L. ZIRBEL (1997) Translation and dispersion of mass by isotropic Brownian flows. *Stochastic Processes and their Applications*, **70**: 1-29.
- [27] R.E. DAVIS (1983) Oceanic Property Transport, Lagrangian Particle Statistics, and their Prediction. *Journal of Marine Research*, **41**: 163-194.

**Table 1.** Effective dispersion constant and single particle diffusivity

t	0.01	0.1	1	10
$K_d$	4.28	0.34	0.034	0.0034
$K$	5.05	0.44	0.039	0.0046

**Table 2.** Particle pair and single particle diffusivities

t	0.01	0.1	1	10
$K_p$	4.97	0.39	0.037	0.0042
$K$	5.05	0.44	0.039	0.0046

## Figure Captions

**Figure 1.** The variance of the centroid versus time

- a)**  $t=0.01, c=10, l=10, a$  is Unif(-54,54)    **b)**  $t=0.1, c=0.1, l=0.1, a$  is Unif(-5.4,5.4)  
**c)**  $t=1, c=0.01, l=0.01, a$  is Unif(-0.54,0.54)    **d)**  $t=10, c=1, l=0.1, a$  is Unif(-0.17,0.17).

**Figure 2.** The trace of the dispersion matrix versus time

- a)**  $t=0.01, c=10, l=10, a$  is Unif(-54,54)    **b)**  $t=0.1, c=0.1, l=0.1, a$  is Unif(-5.4,5.4)  
**c)**  $t=1, c=0.01, l=0.01, a$  is Unif(-0.54,0.54)    **d)**  $t=10, c=1, l=0.1, a$  is Unif(-0.17,0.17).

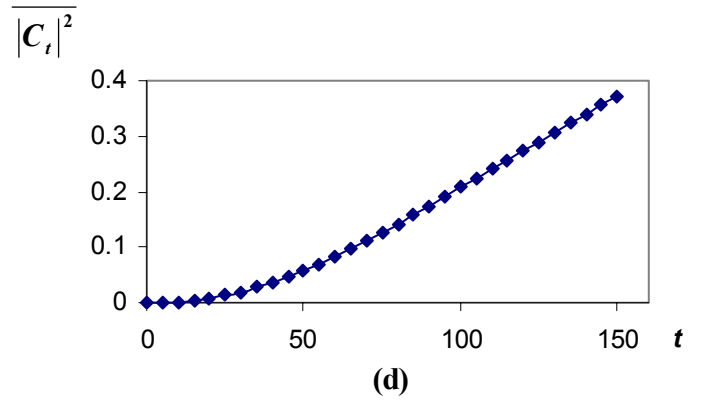
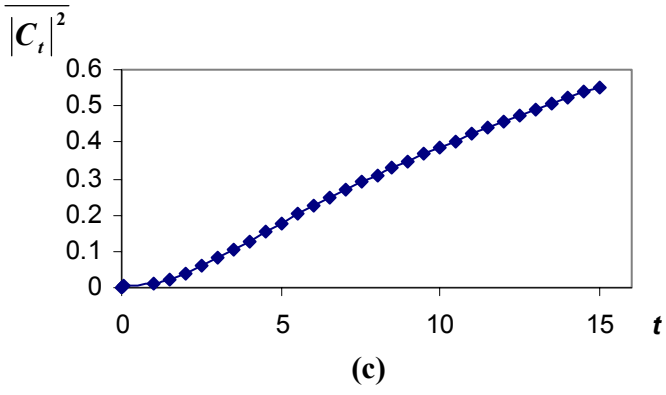
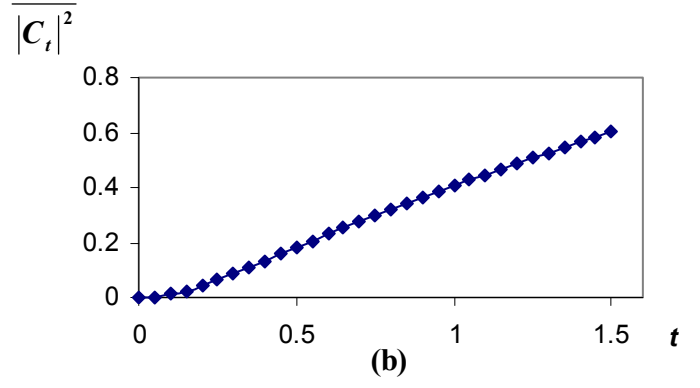
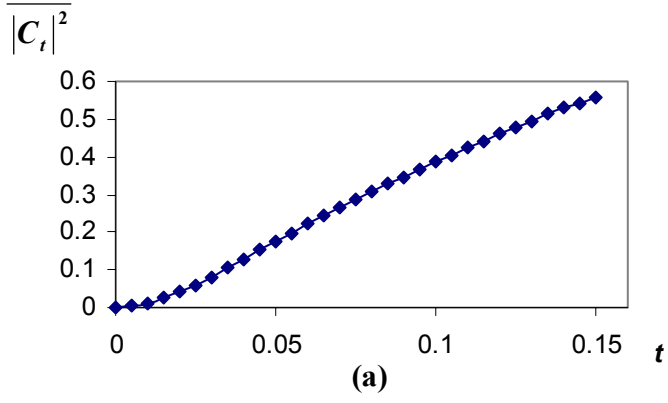
**Figure 3.** The radius of the minimal circle versus time

- a)**  $t=0.01, c=10, l=10, a$  is Unif(-54,54)    **b)**  $t=0.1, c=0.1, l=0.1, a$  is Unif(-5.4,5.4)  
**c)**  $t=1, c=0.01, l=0.01, a$  is Unif(-0.54,0.54)    **d)**  $t=10, c=1, l=0.1, a$  is Unif(-0.17,0.17).

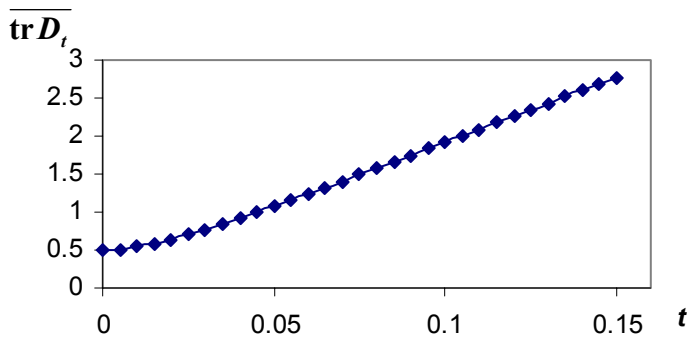
**Figure 4.** Particle pair separations versus time. In each plot, the curves go from smallest to largest initial separation from bottom to top.

- a)**  $t=0.01, c=10, l=10, a$  is Unif(-54,54)    **b)**  $t=0.1, c=0.1, l=0.1, a$  is Unif(-5.4,5.4)  
**c)**  $t=1, c=0.01, l=0.01, a$  is Unif(-0.54,0.54)    **d)**  $t=10, c=1, l=0.1, a$  is Unif(-0.17,0.17).

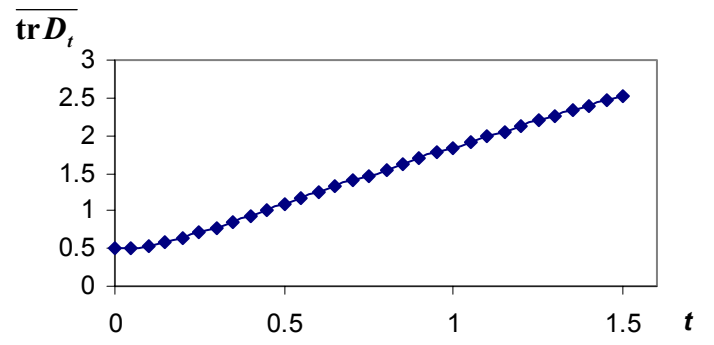
**Figure 5.** Log-log plot of the effective dispersion constant  $K_d$  and the particle pair diffusivity  $K_p$  with respect to the time scale  $t$ .



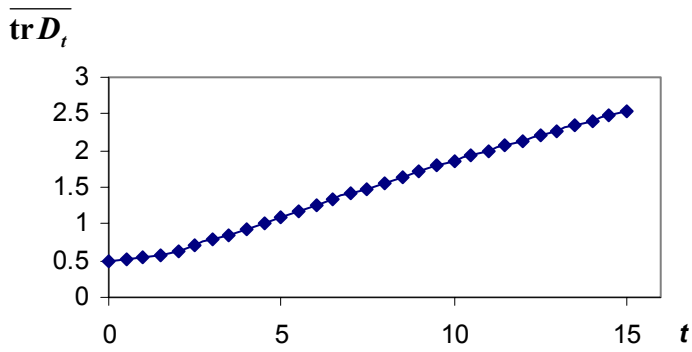
Çağlar, Figure 1.



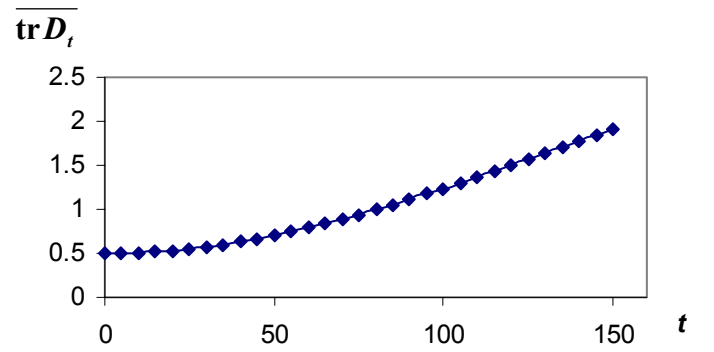
(a)



(b)

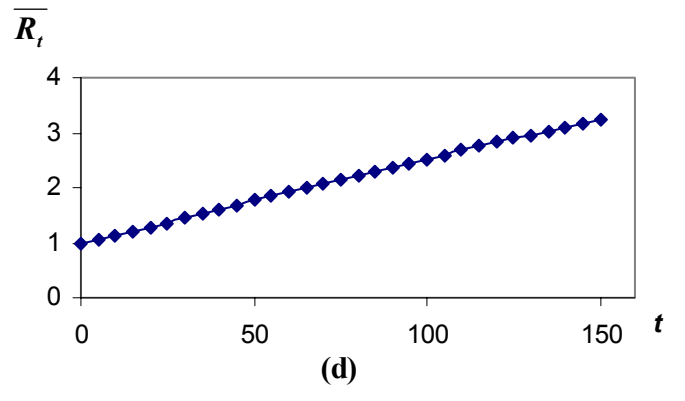
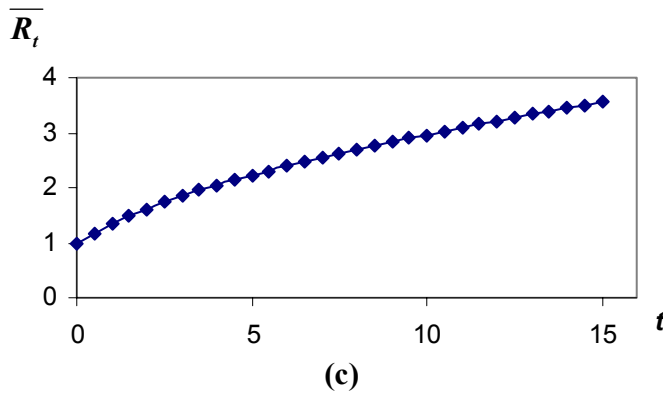
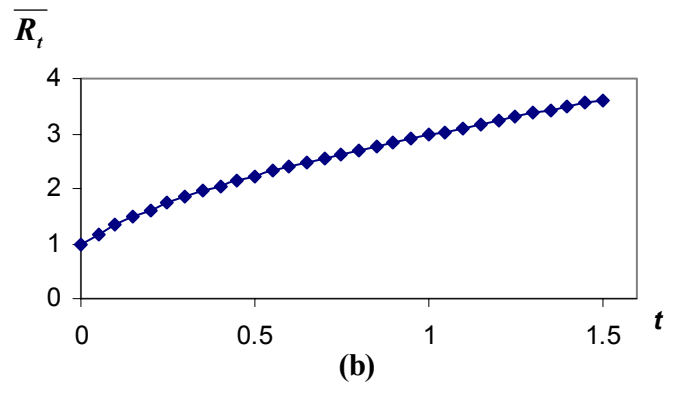
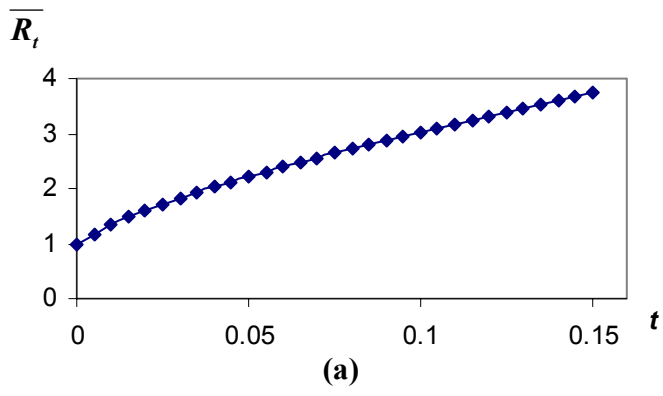


(c)

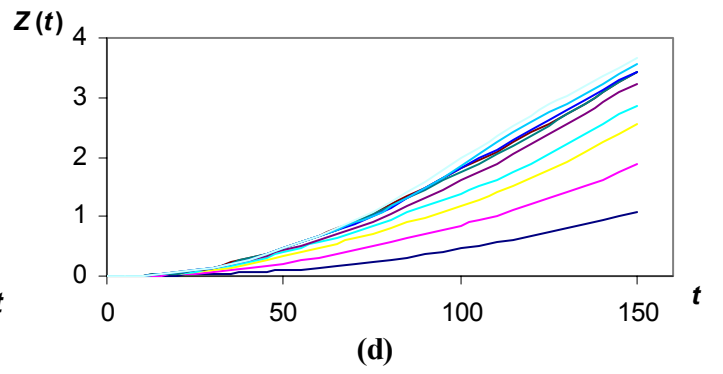
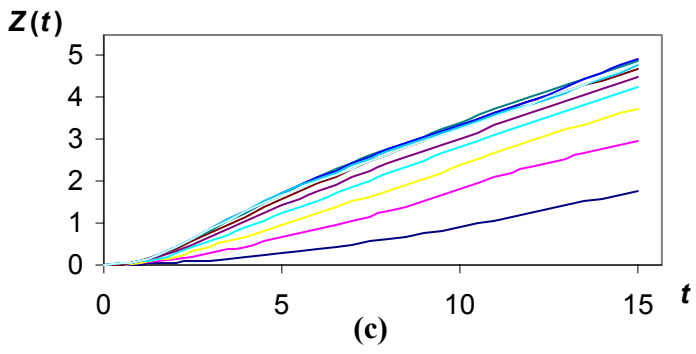
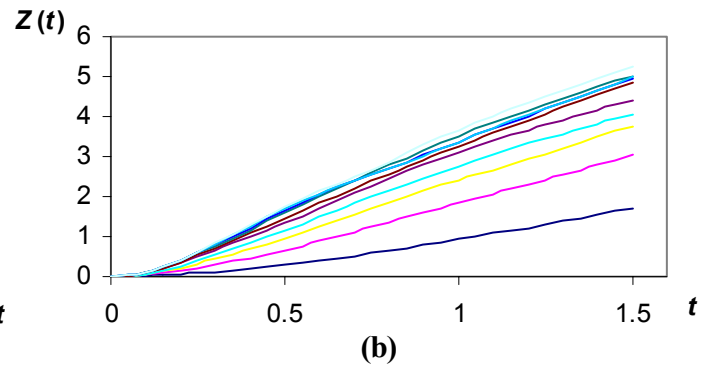
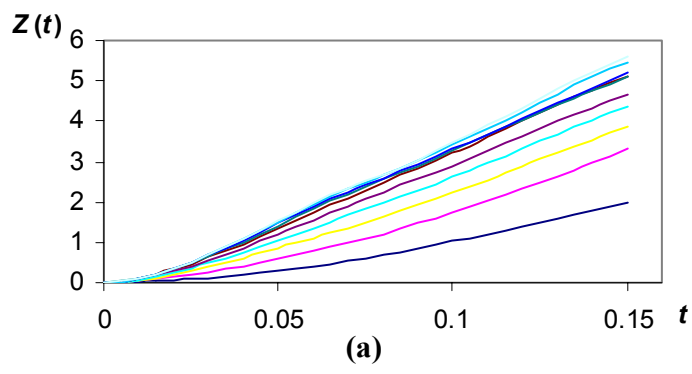


(d)

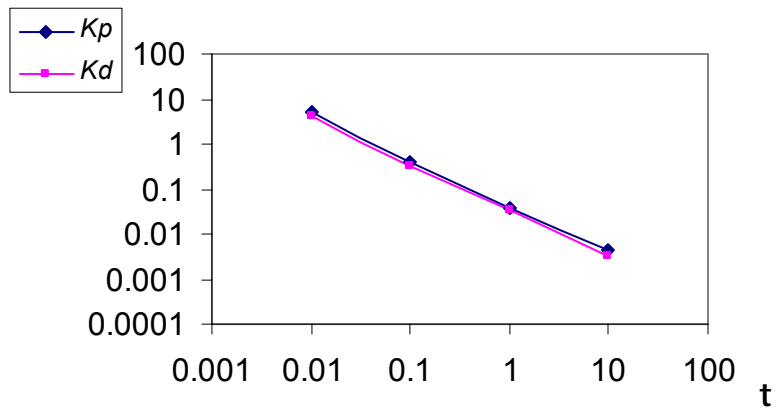
Çağlar, Figure 2.



Çağlar, Figure 3.



Çağlar, Figure 4.



Çağlar, Figure 5.